



**HAL**  
open science

# Computational investigation on CO<sub>2</sub> capturing capacity of N-doped and Na-decorated Graphdiyne

M. Asgari Bajgirani, Z. Biglari, Mehdi Sahihi

► **To cite this version:**

M. Asgari Bajgirani, Z. Biglari, Mehdi Sahihi. Computational investigation on CO<sub>2</sub> capturing capacity of N-doped and Na-decorated Graphdiyne. *Fuel*, 2023, 345, pp.128169. 10.1016/j.fuel.2023.128169 . hal-04048875

**HAL Id: hal-04048875**

**<https://uca.hal.science/hal-04048875v1>**

Submitted on 28 Mar 2023

**HAL** is a multi-disciplinary open access archive for the deposit and dissemination of scientific research documents, whether they are published or not. The documents may come from teaching and research institutions in France or abroad, or from public or private research centers.

L'archive ouverte pluridisciplinaire **HAL**, est destinée au dépôt et à la diffusion de documents scientifiques de niveau recherche, publiés ou non, émanant des établissements d'enseignement et de recherche français ou étrangers, des laboratoires publics ou privés.



Distributed under a Creative Commons Attribution - NonCommercial - NoDerivatives 4.0 International License

1 **Computational Investigation on CO<sub>2</sub> Capturing Capacity**  
2 **of N-doped and Na-decorated Graphdiyne**

3  
4 **M. Asgari Bajgirani<sup>a</sup>, Z. Biglari<sup>a,\*</sup>, M. Sahihi<sup>b,\*</sup>**

5 *<sup>a</sup> Department of Physical Chemistry, Faculty of Chemistry, University of Lorestan, Lorestan, Iran*

6 *<sup>b</sup> Université Clermont Auvergne, CNRS, Clermont Auvergne INP, Institut de Chimie de Clermont-*  
7 *Ferrand, F-63000 Clermont-Ferrand, France*

8  
9  
10  
11  
12  
13  
14  
15  
16  
17 **\*Corresponding authors**

18 Zeinab Biglari and Mehdi Sahihi

19 Email: [biglari.z@lu.ac.ir](mailto:biglari.z@lu.ac.ir) and [mehdi.sahihi@uca.fr](mailto:mehdi.sahihi@uca.fr)

20 Tel.: +33 (0) 473407384

21 **Abstract**

22 Graphdiyne (GDY) is a newly discovered member of the two-dimensional carbon allotropes  
23 that has been proposed as a material for carbon dioxide (CO<sub>2</sub>) capture and storage technology.  
24 The GDY structure is composed of several hybridized carbon atoms, and despite its superior  
25 electronic capabilities, modifying its structure can facilitate the advancement of its practical  
26 applications. This study considered, N-doping, Na-decoration, and their combinations as GDY  
27 modifications. The dispersion-corrected density functional theory (DFT-D2) approach was  
28 used to investigate the structural and electronic properties of the resultant adsorbents and their  
29 CO<sub>2</sub> adsorption behavior. Among three different N-doped structures, substituting an N atom  
30 for the Carbon with hybridization of SP<sup>2</sup>-SP (C<sub>SP<sup>2</sup>-SP</sub>) produced the most stable N-doped GDY  
31 with E<sub>coh</sub> = -7.23eV. Four different locations of GDY were decorated by Na atom, and the  
32 center of the H3 was identified as the most stable site with E<sub>ads</sub> = -3.804eV. This site was also  
33 the most favorable for Na decorating of the N-doped GDY, with E<sub>ads</sub> = -3.347eV. Moreover,  
34 the results indicated that when a single CO<sub>2</sub> was adsorbed on the Na-decorated GDY, the  
35 adsorption energy was -0.432eV, the highest value among the pristine and modified structures.  
36 However, evaluation of the maximum CO<sub>2</sub> capturing capacity of the systems revealed that N-  
37 doped GDY could capture eleven CO<sub>2</sub> molecules, ca. 68.92 Wt%, which makes it a potential  
38 candidate for future CO<sub>2</sub> capture, storage, detection, and removal applications.

39

40

41

42

43 **Keywords:** Graphdiyne (GDY), CO<sub>2</sub> capture, 2D carbon allotropes, Adsorption, DFT-D2.

## 44 **1. Introduction**

45 Modern industry is quickly evolving, and rising levels of CO<sub>2</sub> in the atmosphere necessitate  
46 the development of industrial systems for capturing and storing CO<sub>2</sub> along with other  
47 greenhouse gases (e.g., CO, CH<sub>4</sub>, and NO<sub>2</sub>) [1,2]. CO<sub>2</sub> capturing systems have utilized two-  
48 dimensional (2D) carbon-based materials such as graphene and graphyne [3–6]. Like the other  
49 members of the 2D carbon family, GDY has fascinating physicochemical features and is  
50 frequently employed in academic research [7–10]. The GDY's  $\pi$ -conjugated structure  
51 comprises of carbon hexagonal rings joined by diacetylene bridges (-C $\equiv$ C-C $\equiv$ C-), in which the  
52 sp-sp<sup>2</sup> hybridized carbon atoms serve as active sites. GDY has superior activity and selectivity  
53 compared to graphene, making it a suitable material for developing CO<sub>2</sub> capture techniques  
54 [11].

55 In 2010, Li et al. employed hexaethynylbenzene to synthesize GDY on a Cu foil surface via a  
56 cross-coupling process [12]. Due to its physicochemical qualities, there are various applications  
57 for GDY, including lithium-ion batteries, photocatalysis, electronic systems, energy storage,  
58 electrode materials, and hydrogen purification systems [8–10,13,14]. CO<sub>2</sub> capture capabilities  
59 of GDY are affected by many ways of tuning the structure, such as imposing defects, atom  
60 doping, and decorating [15,16]. The atom-doped GDY exhibits different charge transport, band  
61 gap, Fermi-level, and thermal stability than pristine GDY. In the literature, atoms such as B, P,  
62 N, and S have been utilized to prepare various kinds of doped GDY [10,17–19]. Wu et al.  
63 studied the performance of pristine and N-/B-doped GDY for detecting hazardous and  
64 greenhouse gases. They found that B-doped GDY had more sensitivity and selectivity for NO,  
65 NO<sub>2</sub>, and NH<sub>3</sub> than pristine and N-doped GDY [16].

66 The decorating of metal atoms is another exciting method for improving the gas adsorption  
67 ability of GDY. Decorating atoms such as alkali, alkaline earth metals, and transition metals

68 can affect electron mobility by converting GDY from a narrow band-gap semiconductor to a  
69 semi-metallic state [20]. Using density functional theory (DFT) calculations, Feng et al.  
70 anchored Cu on B- and N-doped GDY to study the influence of decoration on electronic  
71 structures and CO<sub>2</sub>-reduction reaction catalytic performance. Comparing the adsorption  
72 energies and charge transfer, they found that the Cu@N-doped GDY monolayer performs  
73 better for CO<sub>2</sub> reduction than the Cu@B-doped GDY monolayer [21].

74 Zou et al. investigated the effect of anchoring various transition metal atoms on the stability,  
75 electronic, and magnetic characteristics of N-doped GDY. They observed that electron mobility  
76 was increased, the metal atom binding strength was improved, and the stability of metal-  
77 decorated GDY was boosted. They also reported that Fe@2N-GDY provides the best catalytic  
78 performance with the lowest CO oxidization energy barrier [5]. Ebadi et al. studied the  
79 influence of Ca-decoration on the electronic and structural characteristics of GDY, and the  
80 adsorption behavior of H<sub>2</sub> molecules on pristine and Ca-decorated GDY, using DFT  
81 calculations. They concluded that calcium-decorated GDY is viable for hydrogen storage  
82 applications [20]. They also explored the adsorption behavior of methanol and CO molecules  
83 on intact GDY and Ca-GDY using DFT-D2 simulations. Their findings indicated that Ca-GDY  
84 might be a viable candidate for practical applications such as methanol and CO molecule  
85 capturing and storage [15]. Metal atoms have also been decorated on other 2D adsorbents to  
86 improv their adsorption of CO<sub>2</sub>. Using DFT-D3 simulations, Darvishnejad et al. studied the  
87 effect of Sr, Sc, and Cr decoration on graphyne's structural and electronic characteristics of  
88 enhance CO<sub>2</sub> capture capacity. They investigated the adsorption energies of systems by placing  
89 the metal atoms at various locations of the graphyne frame. For CO<sub>2</sub> adsorption on the  
90 structures, the most stable modified structures were utilized as the adsorbent [4,22].

91 Yang et al. crafted a hetero junction composed of Bi<sub>2</sub>WO<sub>6</sub> and GDY nanosheets and  
92 investigated the photo reduction CO<sub>2</sub> activity under simulated sunlight irradiation [23]. Their

93 findings indicated that the overall CO<sub>2</sub> conversion over the 2D/2D GDY/Bi<sub>2</sub>WO<sub>6</sub> is 4.9 times  
94 higher than Bi<sub>2</sub>WO<sub>6</sub>. This was attributed to higher light adsorption, conductivity, and a wide  
95 interfacial contact area of the GDY, ensuring the improvement in photo-induced charge  
96 separation rates. They also claimed that the CO<sub>2</sub> adsorption of the hybrid structure was  
97 enhanced due to the increased specific surface area and micropores [23]. Dang et al. presented  
98 a computational method for generating a set of GDY-based frameworks, GDY-Rs and  
99 Li@GDY-Rs [24]. In the building blocks of GDY, they incorporated several functional groups  
100 (R: NH<sub>2</sub>, OH, COOH, and F) and the doping metal atom (Li). Finally, a screening was carried  
101 out to identify the top candidates for CO<sub>2</sub> capture and sequestration applications. The combined  
102 DFT and grand canonical Monte Carlo (GCMC) simulations were used to examine the pore  
103 structure and morphology and the CO<sub>2</sub> adsorption and separation properties of these  
104 frameworks. They reported that the combination of Li-doping and hydroxyl group grafting  
105 results in an unanticipated synergistic effect for effective CO<sub>2</sub> capturing, with a CO<sub>2</sub> uptake of  
106 4.83 mmol/g (at 298 K and 1 bar). They recommended Li@GDY-OH as one of the most  
107 promising materials for CO<sub>2</sub> capture and separation, with a selectivity of 13 for CO<sub>2</sub> over CH<sub>4</sub>  
108 (at 298 K and 1 bar) [24]. GDY's particular high  $\pi$  hybrid structure gives it uniform nanohole  
109 distribution, nonuniform electron distribution, excellent electrical conductivity and electron  
110 mobility, tunable band gaps, and high chemical stability. These attractive properties make  
111 graphdiyne a promising candidate for producing high-performance products and, as a  
112 combination for CO<sub>2</sub>-capturing, a good candidate for photocatalytic solar fuel production and  
113 etcetera [25].

114 As mentioned above, the N-doped GDY exhibits different charge transport, band gap, Fermi-  
115 level, and thermal stability than pristine GDY [10,17–19]. Also, decorating the alkali metal  
116 atoms can improve the gas adsorption ability of GDY [20]. Hence, combining these two  
117 modifications may improve the CO<sub>2</sub> capturing property of GDY. To the best of our knowledge,

118 there is no detailed investigation about CO<sub>2</sub> capturing properties of N-doped and alkali metal-  
119 decorated GDY. Therefore, in the present study, three sorts of alterations were made to the  
120 GDY structure to propose a candidate for CO<sub>2</sub> capture and storage (CCS) technology, and  
121 exciting results were observed. We explored various GDY atoms and sites to discover the  
122 optimal position for doping the N atom and decorating the Na atom. The optimal configuration  
123 of the modified structures, which included N-doped, Na-decorated, and Na-decorated N-doped  
124 GDY, was then determined using the cohesive energy and metal atom adsorption energy. The  
125 structural and electronic properties of the best structures and their behavior in the adsorption  
126 of single and multiple CO<sub>2</sub> molecules were investigated. Finally, each structure's maximum  
127 CO<sub>2</sub> adsorption capacity was estimated to determine the structure with the best performance.  
128 Since most of the previously published research on CO<sub>2</sub> adsorption on GDY has focused on  
129 GDY decorated with transition metals, we hope that the novelty of the present study (using the  
130 alkali metals decorated GDY) could shed light in the CO<sub>2</sub> capturing and storage technologies.

## 131 **2. Computational methods**

132 The structural and electronic characteristics of pure and modified GDY structures, as well as  
133 their CO<sub>2</sub> adsorption properties, are examined in this study. First, several Na-decorated and N-  
134 doped GDY initial configurations were created and relaxed to determine the most stable  
135 geometry. The spin-polarized DFT approach was used for all calculations, including geometry  
136 optimization, Na adsorption, electronic properties, CO<sub>2</sub> capture, and charge distribution. The  
137 generalized gradient approximation (GGA) level of theory with the Perdew-Burke-Ernzerhof  
138 (PBE) [26] was used as the exchange-correlation functional. The double numerical plus  
139 polarization (DNP) basis set [27] was employed in the calculation using the DMol3 module  
140 [28], which is comparable with the 6-31G(d,p) basis set regarding computational accuracy [29].  
141 The DFT-D2 approach, which was developed by Grimme, was utilized to account for  
142 dispersive inter-molecular interactions and long-range Van der Waals forces [30–32]. A 2×2×1

143 supercell of GDY unit cell with a vacuum space of 20 Å in the z-direction was built to avoid  
 144 the interactions between layers. Integrations in the Brillouin zone were carried out using a  
 145 7×7×1 gamma-centered Monkhorst-Pack mesh of k-grid sampling. No symmetry limitations  
 146 were imposed in geometry optimization, and all atoms were relaxed. The convergence  
 147 tolerance for energy accuracy, maximum force, displacement, and global orbital cut-off radius  
 148 was selected as 10<sup>-5</sup> Ha, 2×10<sup>-3</sup> Ha/Å, 5×10<sup>-3</sup> Å, and 5.1 Å, respectively. Different parameters  
 149 and diagrams like band structure, the density of State (DOS), partial DOS (PDOS), total DOS  
 150 (TDOS), charge density, and Hirshfeld atomic charges were also presented for qualitative and  
 151 quantitative interpretations of results.

152 The stability of N-doped GDY structures was determined by cohesive energy ( $E_{coh}$ ) that can be  
 153 calculated by Eq. 1 [29]:

$$E_{coh} = \frac{E_{N-dopedGDY} - n_C E_C - n_N E_N}{n_C + n_N} \quad (1)$$

154 where  $E_{N-doped GDY}$ ,  $E_C$ , and  $E_N$  are the total energy of N-doped GDY, isolated carbon, and  
 155 Nitrogen atoms,  $n_C$  and  $n_N$  are the numbers of carbon and nitrogen atoms, respectively. The  
 156 adsorption energy ( $E_{ads}$ ) of the Na atom adsorbed on the GDY sheet is calculated using Eq. 2  
 157 [4]:

$$E_{ads}^{Na} = E_{Na-decorated(N-doped)GDY} - E_{pristine(N-doped)GDY} - E_{Na} \quad (2)$$

158 where  $E_{Na-decorated (N-doped)GDY}$ ,  $E_{pristine(N-doped)GDY}$ , and  $E_{Na}$  are the total energy of Na-decorated  
 159 (N-doped) GDY, pristine (N-doped) GDY, and isolated Na atom, respectively. The average  
 160 adsorption energy ( $E_{ads}$ ) and the adsorption energy ( $E_s$ ) per CO<sub>2</sub> molecule of each step are given  
 161 by Eq. 3 and Eq. 4, respectively:



$$E_{ads} = \frac{1}{n} (E_{GDY-Na/N-nCO_2} - E_{GDY-Na/N} - nE_{CO_2}) \quad (3)$$

$$E_s = E_{GDY-Na/N-nCO_2} - E_{GDY-Na/N-(n-1)CO_2} - E_{CO_2} \quad (4)$$

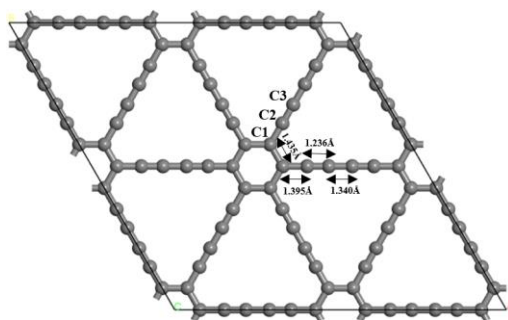
162 where  $E_{GDY-Na/N-nCO_2}$ ,  $E_{GDY-Na/N-(n-1)CO_2}$ ,  $E_{GDY-Na/N}$ , and  $E_{CO_2}$  are the total energy of the system  
 163 containing the modified GDY and  $nCO_2$ , the system containing modified GDY and  $(n-1)CO_2$ ,  
 164 the modified GDY, and isolated  $CO_2$  molecule, respectively and  $n$  is the number of the  
 165 adsorbed  $CO_2$  molecules.  $E_s$  shows the adsorption energy of the  $n^{th}$   $CO_2$  onto the structure of  
 166  $(n-1)^{th}$  step. Upon the value of  $E_s$  becoming smaller than 0.1eV, the adsorbent no longer has  
 167 the sufficient ability to adsorb the subsequent  $CO_2$  molecule [4]. Then, the addition of  $CO_2$   
 168 molecules to the adsorbent is stopped.

169  $CO_2$  capture capacity was calculated using the following equation:

$$CO_2 \text{ capture capacity (wt.\%)} = \left[ \frac{M_{CO_2}}{M_{CO_2} + M_{host}} \right] \times 100 \quad (5)$$

170 where  $M_{CO_2}$  and  $M_{host}$  are the total mass of the adsorbed  $CO_2$  molecules and the mass of the  
 171 adsorbent.

172 As shown in **Fig. 1**, the symmetric structure of GDY composes of an  $sp^2$ -hybridized hexagonal  
 173 carbon ring and six  $sp$ -hybridized acetylenic carbon chains [20]. There are three types of carbon  
 174 atoms in the structure: C1( $C_{SP^2-SP^2}$ ), C2( $C_{SP^2-SP}$ ), and C3( $C_{SP-SP}$ ) due to their different types of  
 175 hybridization. The position of each of these structural carbons and the length of the bonds  
 176 connecting them were illustrated in **Fig. 1**. To improve the  $CO_2$  adsorption capability of the  
 177 structure, the GDY structure was modified, and the electronic and structural effects of the  
 178 modifications were investigated. On pure GDY, Discrete structural modifications such as N-  
 179 doping and Na-decoration were done in different places on the GDY sheet.



180

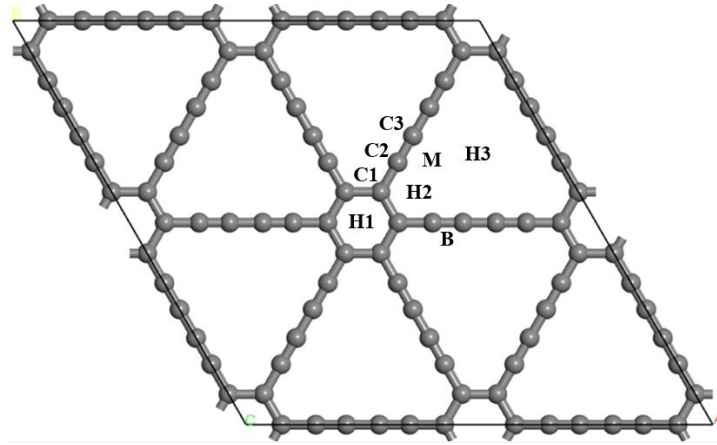
181 **Fig. 1.** The optimized structures of pristine GDY with various C-C bond lengths.

182

### 183 3. Result and discussion

#### 184 3.1. Evaluation of the structural and electronic properties of pristine and modified GDY

185 In the  $2 \times 2 \times 1$  supercell structure of GDY, there are 72 carbon atoms. Unlike graphene, as a  
 186 conductor, GDY has a non-zero band gap at the gamma point ( $\Gamma$ ) [33] and is hence a  
 187 semiconductor. Structural symmetry of GDY can lead to electronic symmetry; applying  
 188 impurities in the structure, such as atom decorating or doping, might induce a deviation from  
 189 this symmetry, improving the gas adsorption capabilities of the adsorbent. Three structural  
 190 alterations were applied to the GDY structure by doping the N atom, decorating the Na atom,  
 191 and combining these two modifications. The places where these alterations are made are shown  
 192 in **Fig. 2**. In the GDY structure; three atomic sites are the candidates for replacement with  
 193 nitrogen atoms (**Fig. 2**). Furthermore, for placing the decorative Na atom, the sites H1, H2, H3,  
 194 and B were chosen. **Table 1** shows the energy released by each modified structure after  
 195 geometry optimization.



196

197 **Fig. 2.** Three types of carbon atoms (C1, C2, and C3) and the five possible sites are labeled by H1, H2, H3, B,  
 198 and M.

199

200

201 **Table 1.** Binding and adsorption energies of modified structures (N doped-, Na decorated-, and Na decorated-N  
 202 doped GDY) at different binding and adsorption sites.

Structure	Cohesive Energy (eV)			Adsorption energy(eV)							
	C1	C2	C3	H1		H2		H3		B	
				d(Å)=0	d(Å)=1.5	d(Å)=0	d(Å)=1.5	d(Å)=0	d(Å)=1.5	d(Å)=1.5	
N-doped	-7.216	<u>-7.231</u>	-7.226	--	--	--	--	--	--	--	
Na-decorated	--	--	--	-2.986	-2.963	-3.805	-3.802	<u>-3.804</u>	-3.797	-3.502	
Na-decorated	--	-7.231	--	-2.759	-2.759	-3.346	-3.344	<u>-3.347</u>	-3.344	-3.334	

203 The pristine and most stable modified structures (N-doped GDY, Na-decorated GDY, and Na-  
 204 decorated-N-doped GDY) are called S1, S2, S3, and S4, respectively, in the following sections.

205 As can be seen, doping the N atom with cohesive energy ( $E_{coh}$ ) of -7.231eV instead of the C2  
 206 carbon atom resulted in the most stable structure among the modified systems. Additionally,  
 207 with adsorption energy ( $E_{ads}$ ) of -3.804eV, decorating the Na atom in the H3 site is the most  
 208 stable decorated structure. Finally, the Na atom was decorated on several sites of the best S2  
 209 structure, and as shown, the H3 site is the best site among the double-modified structures, with

210 an adsorption energy of -3.347 eV. The bond length and structure energy, cohesive energy, gap  
 211 energy ( $E_g$ ), and Fermi level ( $E_f$ ) are reported for the most stable structures in **Table 2**. Also,  
 212 **Fig. 3** represents the optimized geometrical forms.

213 **Table 2.** Structural and electronic properties of pristine GDY and best conformations of the modified GDYs.

Structure	C1-C1(Å)	C1-C2(N)(Å)	C2(N)-C3(Å)	C3-C3(Å)	$E_{coh}$ (eV)	$E_{ads}$ (eV)	$E_g$ (eV)	$E_f$ (eV)
S1	1.236	1.395	1.435	1.340	-7.709	--	0.445	-5.223
S2	1.197	1.347	1.438	1.323	-7.231	--	0.000	-4.906
S3	1.239	1.394	1.435	1.339	--	-3.804	0.000	-4.850
S4	1.209	1.339	1.439	1.315	--	-3.347	0.000	-4.841

214

215

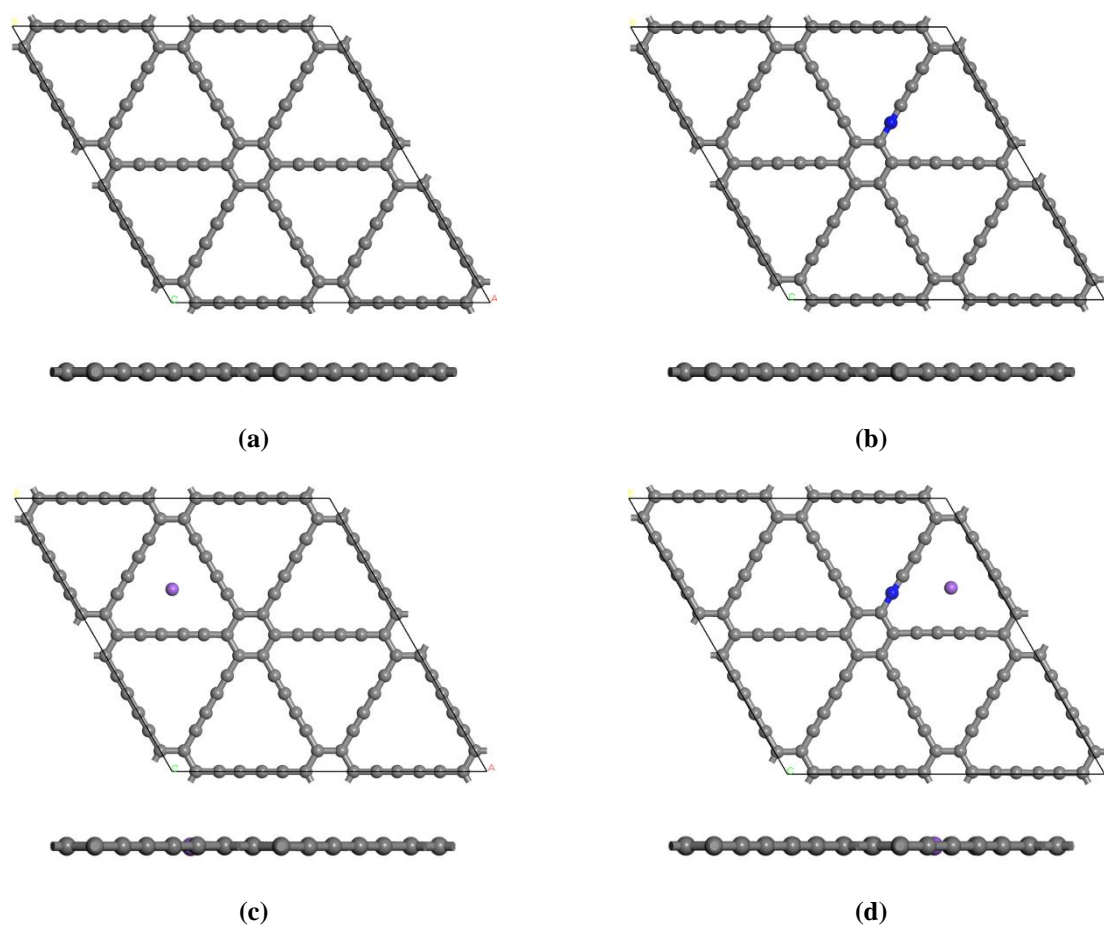


**Fig. 3.** The optimized geometrical structure of (a) pristine GDY and modified GDY (b) S2, (c) S3, and (d) S4. The gray, blue and purple balls represent C, N, and Na atoms, respectively.

216

217 The bond length of nitrogen to the neighboring atoms is directly affected by the smaller radius  
218 of the N atom and the difference in electronegativity between C and N atoms. **Table 2** shows  
219 that in the S2 structure, the length of the C1-C1, C1-N, and C3-C3 bonds reduces while the  
220 length of the N-C3 bond increases. The existence of N-C bonds instead of C-C bonds in the S2  
221 structure and the resulting change in electron distribution can be linked to the decrease in  
222 cohesive energy. An increase in the length of the N-C3 bond can be attributed to the partial  
223 occupation of antibonding orbitals. However, because nitrogen is more electronegative than  
224 carbon, a decrease in the covalent nature of the bond leads to electrostatically stronger N-C  
225 bonds [34,35]. The decorating of Na on the structures S1 and S2 has a minor impact on the  
226 geometrical structure of GDY; this is due to a shift in the charge distribution caused by the  
227 charge donation of the 3s electrons of the Na atom to the  $\pi/\pi^*$  states. Decorating Na on structure  
228 S1 also has higher adsorption energy than decorating Na on structure S2. Graphdiyne, like  
229 graphyne, has sp-hybridized carbons, unlike graphene, which has sp<sup>2</sup>-hybridized carbons. For  
230 this reason, there are  $\pi/\pi^*$  states in the p<sub>x</sub>-p<sub>y</sub> direction in-plane and p<sub>z</sub> orbitals out-of-plane. As  
231 a result, it has  $\pi/\pi^*$  states that can be very effective for creating stronger interactions with metal  
232 and other adsorbing [36,37].

233 The frequency calculations were performed for S2 and S3 structures at different sites (H1, H2,  
234 H3 and B) and at intervals of 0 and 1.5 Å for Na-decorated and N-doped (C1, C2, and C3)  
235 configurations. The results confirm that the best locations for N-doping and Na-decoration are  
236 C2 and H3 sites, respectively (**Table 3**).

237 **Table 3.** The lowest calculated vibrational frequencies ( $\text{cm}^{-1}$ ) related to and N-doped (C1, C2, and C3) and Na-  
 238 decorated in 4 sites (H1, H2, H3 and B).

Structure	Vibrational frequencies ( $\text{cm}^{-1}$ )									
	C1	C2	C3	H1		H2		H3		B
				d(Å)=0	d(Å)=1.5	d(Å)=0	d(Å)=1.5	d(Å)=0	d(Å)=1.5	
S2	29.54	<u>30.88</u>	28.30	---	---	---	---	---	---	---
S3	---	---	---	23.62	21.41	27.19	27.07	<u>31.43</u>	30.18	30.57

239

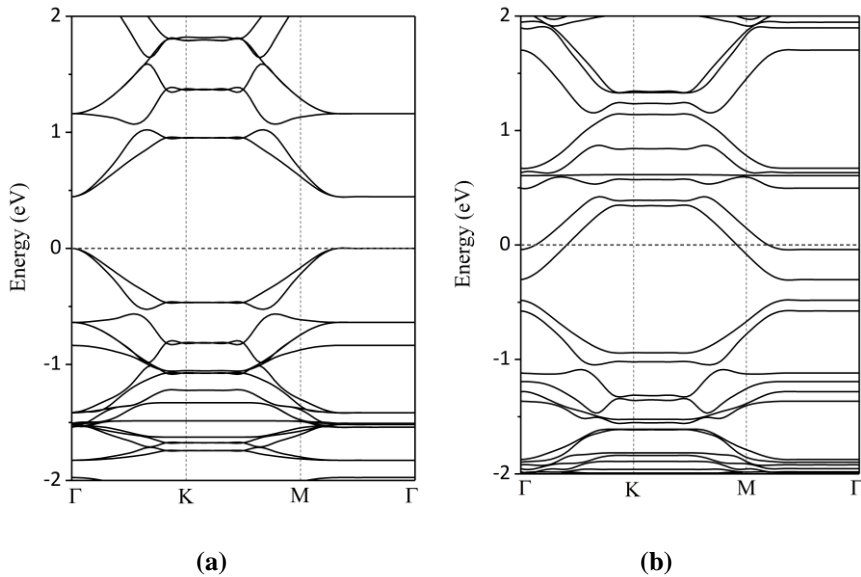
240 As seen in **Table 1**, changes in electronic characteristics cause the band gap to have zero in all  
 241 modified structures. Different band gap values for the GDY structure have been reported in  
 242 theoretical research due to different computational settings, such as different exchange  
 243 correlations. The spin-polarized direct band gap for the GDY monolayer obtained in this study  
 244 is 0.445eV, which agrees with previous theoretical and experimental results [20,38].  
 245 Additionally, **Table 1** indicates that making these modifications increases the Fermi level and  
 246 causes moving towards the conduction band, indicating that the modified structures are n-type  
 247 semiconductors or have improved semi-metallic characteristics [20]. The Fermi level of the S4  
 248 structure shows the most change, confirming its higher conductivity compared to the other  
 249 structures (S1 to S4), which shows that this structure has a higher conductivity than the rest.  
 250 The change in these electronic properties can be justified by examining the electron band  
 251 structure diagram for all four structures, as shown in **Fig. 4**. Pure GDY is a direct semiconductor  
 252 (0.445eV) which is consistent with other previous studies [39], N-doping and Na-decorating  
 253 affected the electron band structure, causing the conduction bands to cross the Fermi energy  
 254 level entirely. Also, the Fermi line has been cut by the conduction bands. This also indicates  
 255 that all modified structures have a semi-metallic electronic character with zero band gap.  
 256 Moreover, the Fermi level is set to zero [29]. Indeed, the presence of nitrogen and alkali metal

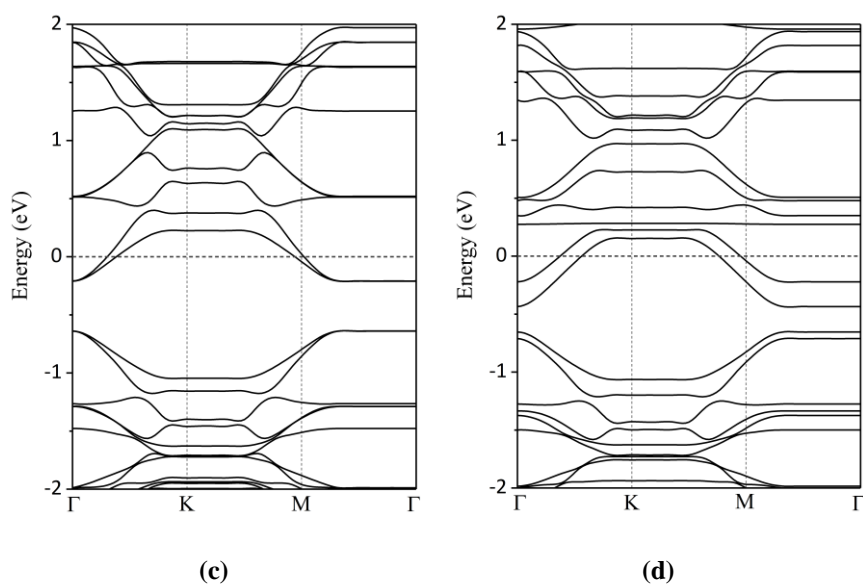
257 atoms causes additional electrons, and a new bonding orbital is created. The energy of this new  
 258 bonding orbital would be between the previous HOMO and LUMO orbitals. Therefore, the  
 259 value of  $E_{\text{gap}}$  is reduced to make GDY a conductive material.

260 The conductivity is exponentially proportional to the value of  $E_{\text{gap}}$ , and the conductivity  
 261 increases with the decrease of  $E_{\text{gap}}$ . The  $E_{\text{gap}}$  value which is a good estimate of conductivity,  
 262 could be calculated using the HOMO-LUMO difference. The electric conductance can be  
 263 related to  $E_{\text{gap}}$  as follows [40]:

$$\sigma \propto e^{-\frac{E_{\text{gap}}}{kT}} \quad (6)$$

264 where  $\sigma$  depicts the electrical conductance,  $k$  is Boltzmann's constant, and  $T$  represents the absolute  
 265 temperature. Thus, at a given temperature, the electrical conductance is inversely proportional to the  
 266  $E_{\text{gap}}$ .





267 **Fig. 4.** Band structure of diagrams: (a) S1, (b) S2, (c) S3, and (d) S4 structures. The Fermi level was set to zero.

268

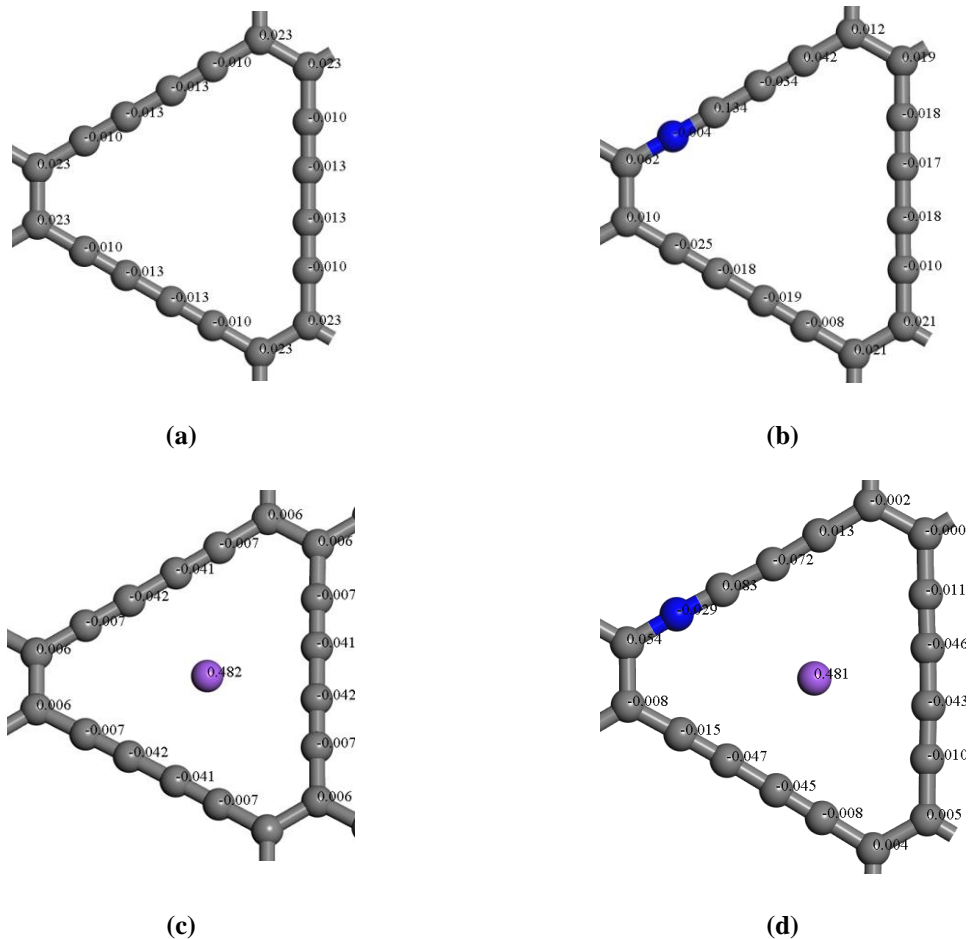
269 The Hirshfeld charges of C1 and C3 atoms, the adjacent atoms of N, changed from  $0.023e^-$  and  
 270  $0.013e^-$  to  $0.062e^-$  and  $0.134e^-$ , respectively, in the S2 structure, as shown in **Fig. 5**. It can be  
 271 inferred that the electron distribution is inclined from the six carbon-ring to the bridge. This  
 272 could be due to the N atom's withdrawing electrons from the carbon skeleton, increasing the  
 273 negative charge of the N atom to  $-0.004e^-$ . The doping of N atoms disrupts the symmetry of  
 274 the electric charge in the structure.

275 Because of the presence of the Na atom, the charge distribution in the entire structure has  
 276 changed, with the positive (negative) charge of C1 (C2) atoms decreasing and the negative  
 277 charge of the C3 atom increasing. After decoration, the charge distribution is transferred from  
 278 the Na atom across the structure, giving this atom a charge of  $+0.482$ . However, the electric  
 279 charge symmetry of the structure is preserved, and only the electric charge values of each atom  
 280 have changed by a certain amount. Carbon atoms C1, C2, and C3 had their electric charge  
 281 values modified from  $0.023e^-$ ,  $-0.010e^-$ , and  $-0.03e^-$  to  $0.006e^-$ ,  $-0.007e^-$ , and  $-0.042e^-$ ,



282 respectively. The quantity of positive charge Na in the S4 structure has changed slightly from  
283 the S3 structure due to the combined effect of doping N and decorating Na.

284



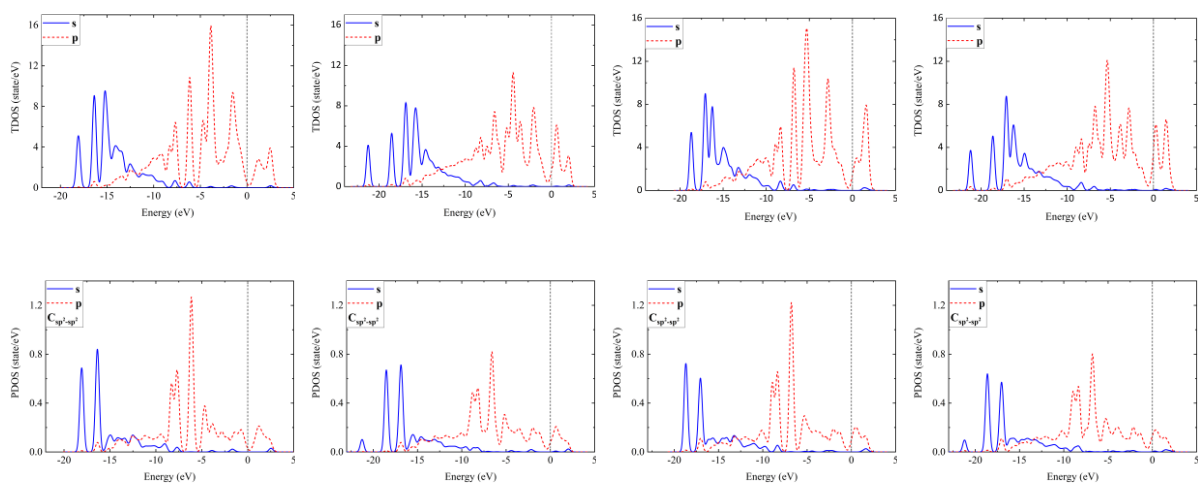
285 **Fig. 5.** Hirshfeld charges of C atoms and modifying atoms (N and Na) in (a) S1, (b) S2, (c) S3, and (d) S4 sites.

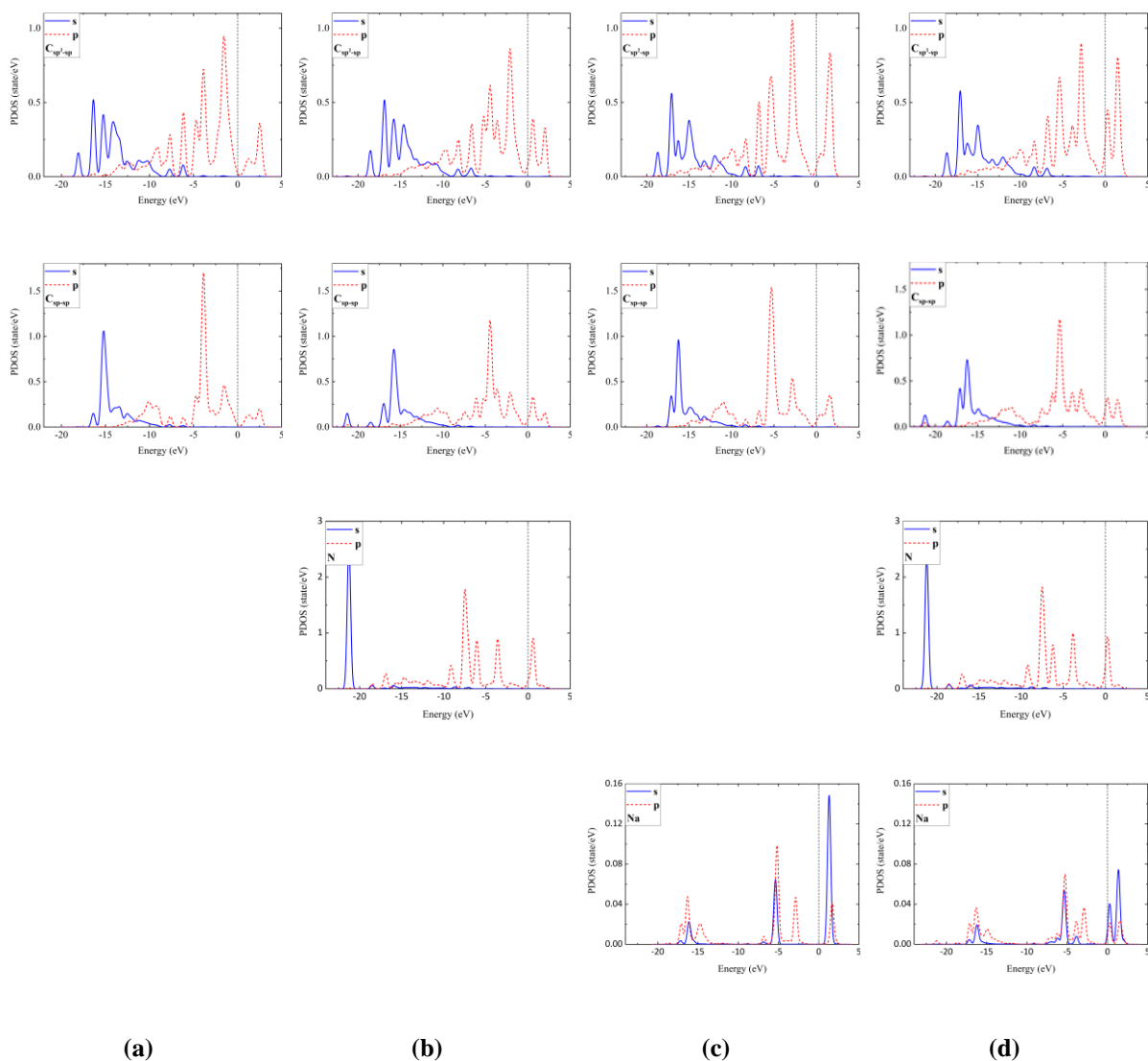
286

287 The TDOS diagram can reveal information about the bonding mechanism, interactions between  
288 the constituent atoms of the structure, contributions of C atoms with various hybridizations,  
289 and charge transfer interaction states. The TDOS and PDOS diagrams for each carbon atom  
290 and the modifying atoms (N, Na) are shown in **Fig. 6**. Fermi level was set to zero in all  
291 diagrams. The contribution of the s- and p-orbitals around the Fermi energy level increases due  
292 to the presence of the N atom with a higher number of electrons in the p-orbital, according to

293 the TDOS diagrams for S1 and S2. The charge density was also broadened at various energy  
 294 levels. Doping N as an impurity in the structure has increased electron density at energy levels  
 295 above the Fermi level. The electronic effect of the adsorption of Na onto the GDY structure  
 296 was along with a low (high) change in the charge density of s-orbital (p-orbital), and charge  
 297 distribution has also shifted towards higher energies. In the decorated structures, the charge  
 298 distribution in the conduction band is increased compared to the S1 structure; this increase is  
 299 higher for the S3 system.

300 The contribution of the p-orbital of the three carbon atoms increases near the Fermi level, as  
 301 shown in the PDOS diagram of **Fig. 6**. The charge density distribution of the GDY in the s-  
 302 orbital is in the energy range of -6 to -20eV, whereas the energy range of S2 is in the range of  
 303 -6 to -22eV. The charge density in the p-orbital of the C1 atom decreases in N-doped structures  
 304 (i.e., S2 and S4). The charge density in the s- and p-orbitals decreases, and the charge density  
 305 is distributed over a broader energy range. Overall, the increase in the charge density in orbitals  
 306 with energies higher than the Fermi level results in the higher electrical conductivity of the S3  
 307 structure. The PDOS diagram of the Na atom in both S3 and S4 structures shows that the charge  
 308 density is lower in S4; this agrees with the electric charge of the atom, implying that Na has  
 309 donated more electric charge to the atoms of the GDY structure.





310 **Fig. 6.** TDOS and PDOS diagrams: (a) S1, (b) S2, (c) S3, and (d) S4.

311

### 312 **3.2. Adsorption of single CO<sub>2</sub> molecule onto the pristine and modified GDY**

313 To find the best site for capturing the single CO<sub>2</sub> molecule on pristine and modified GDY  
 314 structures, the CO<sub>2</sub> molecule was placed horizontally and vertically in different sites, as shown  
 315 in **Fig. 2**. The obtained structures were optimized, and the resulting adsorption energies are  
 316 presented in **Table 4**. The S4 structure provides better adsorption properties among the  
 317 modified structures due to higher adsorption energy. CO<sub>2</sub> is a linear molecule with D<sub>∞h</sub>  
 318 symmetry. During the horizontal interaction with the active sites of the GDY surface, the

319 oxygen atoms could also be placed in front of the active sites. On the other hand, the CO<sub>2</sub>  
 320 molecule was placed horizontally and vertically at various points described above, and the  
 321 system was allowed to calculate the optimized structure by minimizing the energy.

322

323 **Table 4.** Adsorption energy of single adsorbed CO<sub>2</sub> on the pristine and modified GDY at different sites.

Adsorption energy(eV)										
Structure	H1		H2		H3		B		M	
	V	H	V	H	V	H	V	H	V	H
S1	-0.178	-0.181	-0.191	-0.185	-0.270	<u>-0.291</u>	-0.172	-0.174	--	--
S2	-0.161	-0.158	-0.173	-0.268	-0.195	<u>-0.271</u>	-0.218	-0.221	--	--
S3	-0.163	-0.187	-0.285	-0.287	-0.415	<u>-0.432</u>	-0.14	-0.162	--	--
S4	-0.163	-0.178	-0.351	-0.347	-0.439	-0.357	-0.242	-0.233	-0.416	<u>-0.442</u>

324

325 **Table 4** indicates that H3 is the best site for adsorbing CO<sub>2</sub> onto structures S1, S2, and S3,  
 326 while M is the best adsorption site for S4 (the site between H3 and the position of the C2 atom).  
 327 For all the systems (adsorbent + CO<sub>2</sub>), **Table 5** shows the adsorption energy, the length of the  
 328 C-O bonds, the distance of the CO<sub>2</sub> molecule from the adsorbent surface, and the angle O-C-  
 329 O and the charge of each CO<sub>2</sub> atom. The calculated bond length and angle for free CO<sub>2</sub>  
 330 molecule are 1.175Å and 179.66° respectively, which is in line with 1.16Å and 180° from  
 331 experiments[41] and 1.177Å and 179.87° from previous theoretical calculations [42]. As can  
 332 be observed, the C-O bond has a longer bond length when C is close to the adsorbent, and this  
 333 bond length reaches a maximum value in the S4 structure. A single CO<sub>2</sub> molecule adsorbed in  
 334 the closest site (farthest) to the S2 (S3) surface, showing that the CO<sub>2</sub> molecule was affected  
 335 by the attraction (repulsion) force of the N (Na) atom. The effect of repulsion and attraction on  
 336 CO<sub>2</sub> in the S4 structure has resulted in the point between the Na and N atoms being the optimal

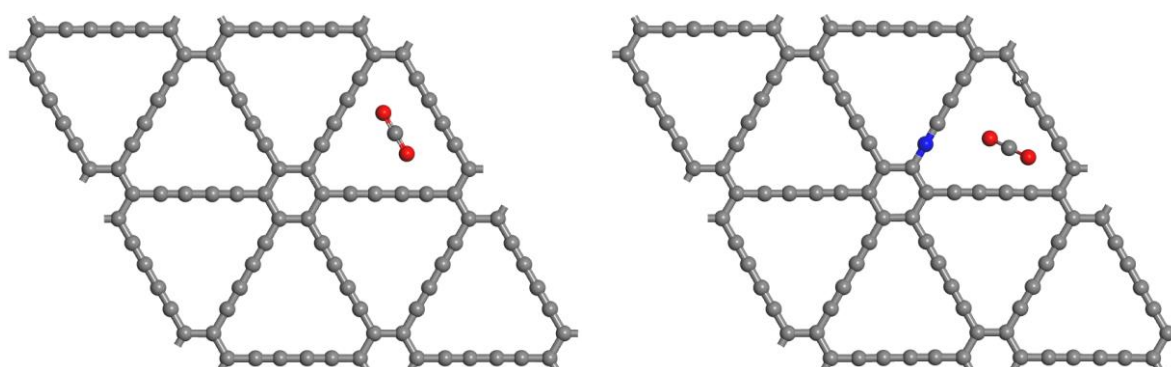
337 site for CO<sub>2</sub> capture onto the structure. Furthermore, comparing the angle of the CO<sub>2</sub> molecules  
 338 reveals that the CO<sub>2</sub> molecule has the biggest angle change in the S2 structure, and the charge  
 339 of the O atom has the highest negative value. When adsorbed on the S3 structure, the carbon  
 340 atom in the CO<sub>2</sub> molecule is most positively charged.

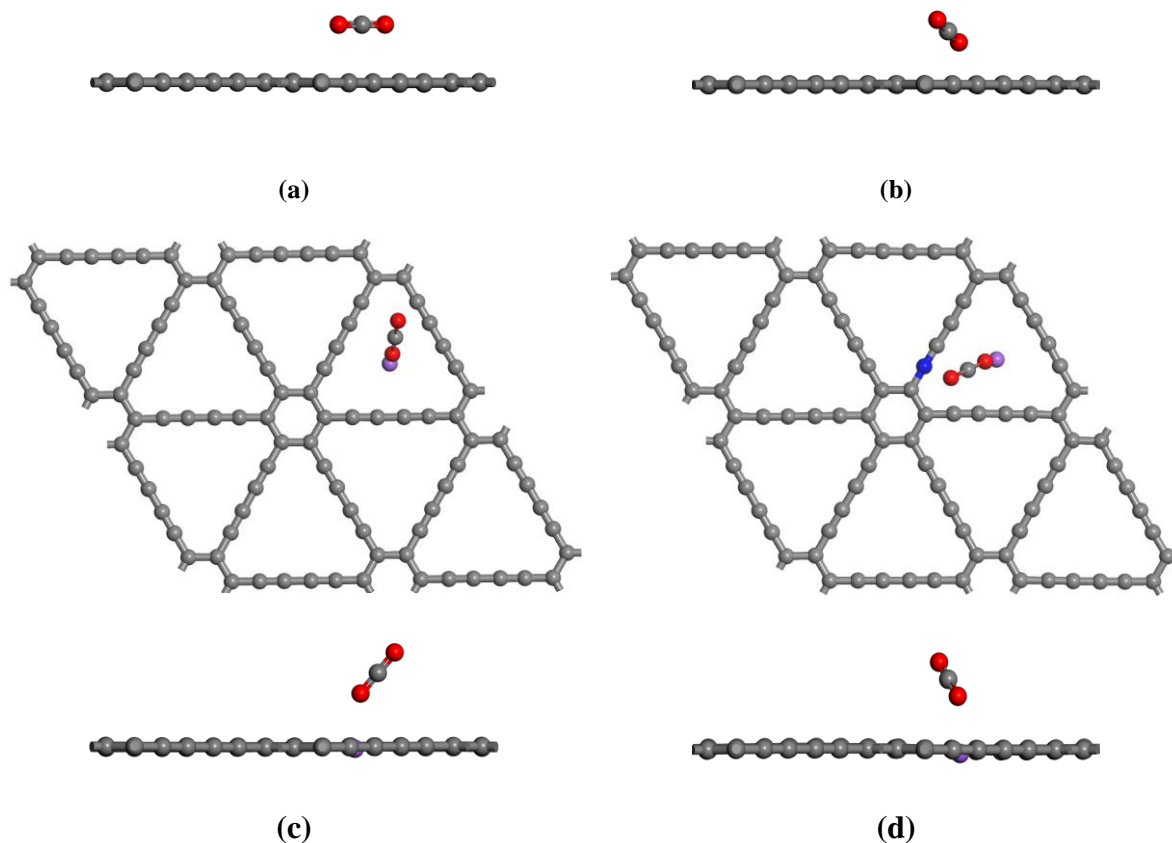
341 **Table 5.** The capture of single CO<sub>2</sub> on the S1, S2, S3, and S4 structures; Adsorption energy ( $E_{\text{ads}}$ ), C-O bond  
 342 length ( $L_{\text{C-O}}$ ), the distance between CO<sub>2</sub> and GDY ( $d$ ), O-C-O angle, and Hirshfeld charge of N, Na and O in CO<sub>2</sub>  
 343 molecule (n: near, f: far from GDY).

structure	$E_{\text{ads}}(\text{eV})$	$L_{\text{C-O}}(\text{\AA})$		$d(\text{\AA})$	$A_{\text{O-C-O}}$	Hirshfeld charges (e)				
		n	f			O(n)	C	O(f)	N	Na
S1	-0.232	1.750	1.75	2.514	179.646°	-0.145	0.29	-0.152	--	--
S2	-0.301	1.176	1.17	2.250	179.173°	-0.159	0.28	-0.149	-0.005	--
S3	-0.432	1.179	1.16	3.189	179.283°	-0.119	0.32	-0.106	--	0.405
S4	-0.391	1.180	1.16	2.864	179.189°	-0.121	0.31	-0.103	-0.025	0.437

344

345 The final spatial orientation and adsorption site of the CO<sub>2</sub> molecule in the structures are shown  
 346 in **Fig. 7**. The CO<sub>2</sub> molecule is horizontal in its most stable state on structure S1; however, it is  
 347 tilted with respect to the adsorbent structure in the modified systems.

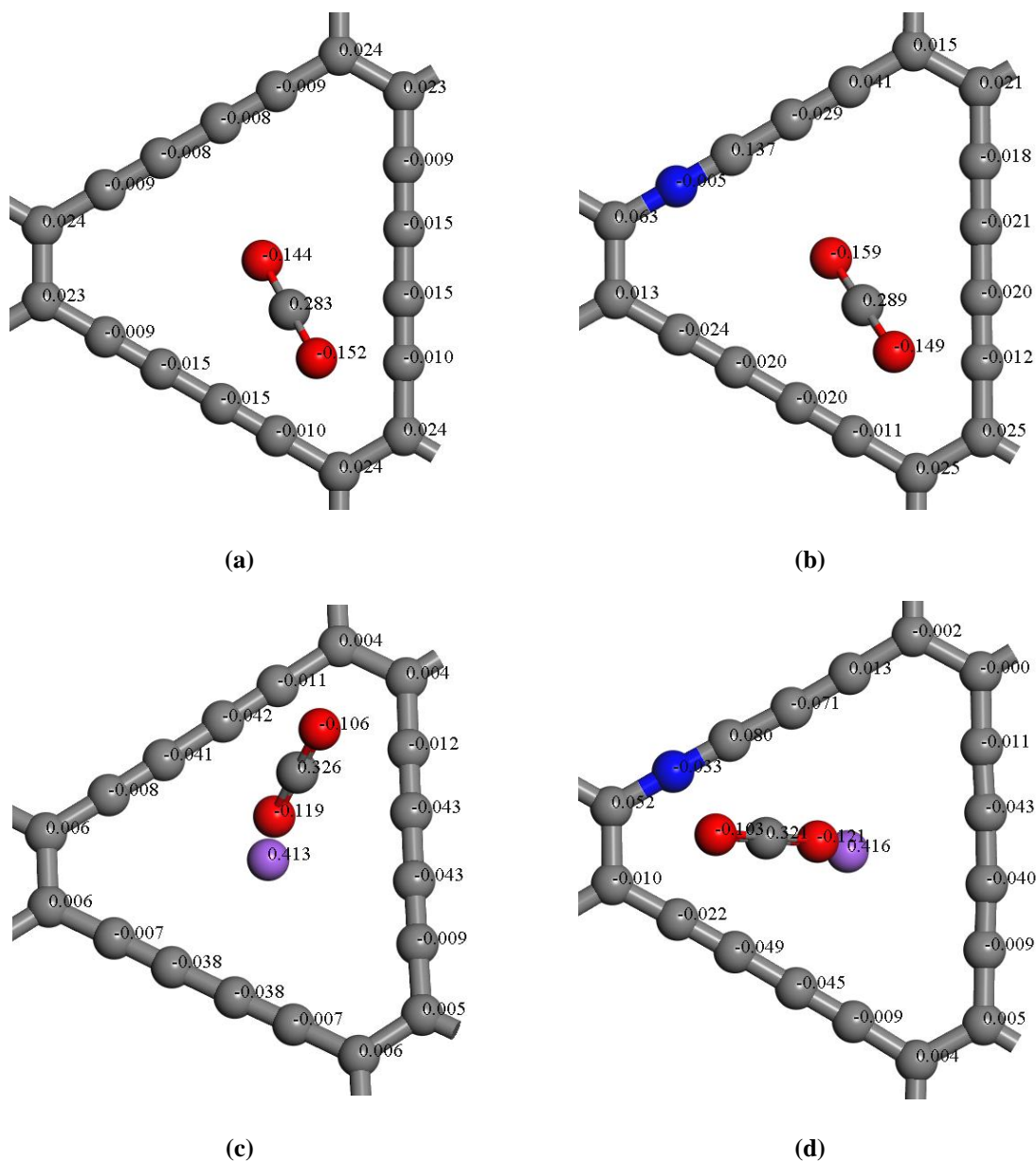




348 **Fig. 7.** Top and side views of the most stable site and orientation of the adsorbed CO<sub>2</sub> onto (a) S1, (b) S2, (c)  
 349 S3, and (d) S4 structures.

350

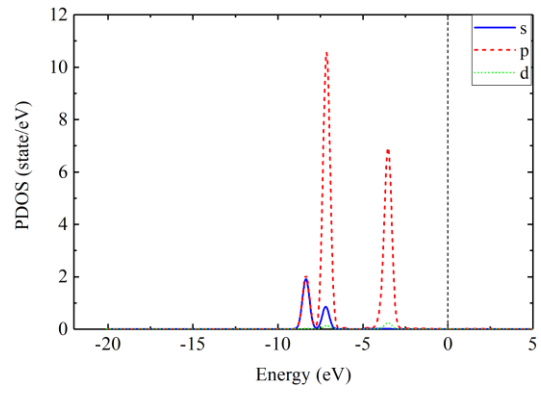
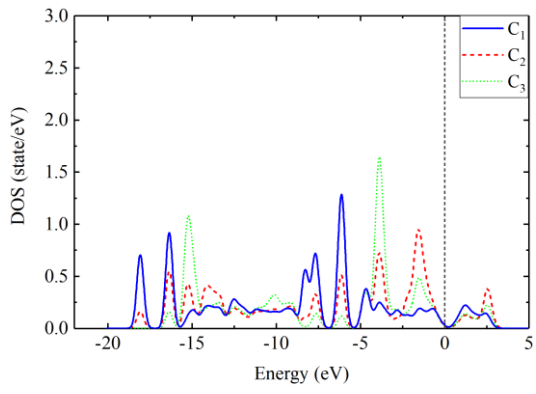
351 The electric charge of each atom in the structure and molecule of CO<sub>2</sub> is shown in **Fig. 8.** The  
 352 charge distribution of the carbon atoms near the gas molecule has changed slightly, as can be  
 353 seen. Because of the difference in Columbic energy and, as a result, the value of adsorption  
 354 energy released, the energy difference impacts structural stability. The nearer O atom to Na  
 355 (N) in the S4 structure has a higher (lower) negative charge. When comparing S3 and S4 (S2  
 356 and S4), we can see that S4 has a more positive (negative) charge on the Na (N) atom.



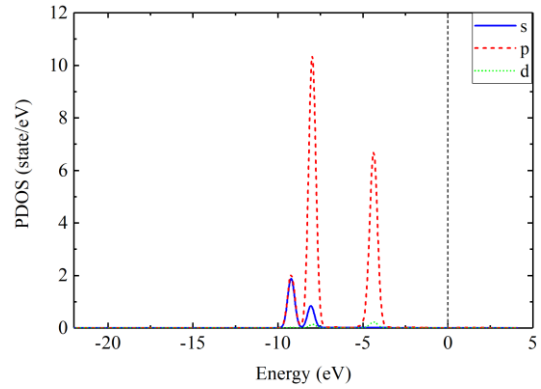
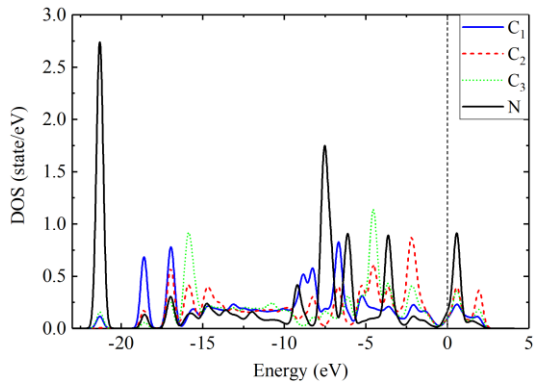
357 **Fig. 8.** Hirshfeld charges of C of structures, modifying atoms (N and Na) and the atoms of the CO<sub>2</sub> molecule in  
 358 (a) S1 (b) S2, (c) S3, and (d) S4 structures.

359

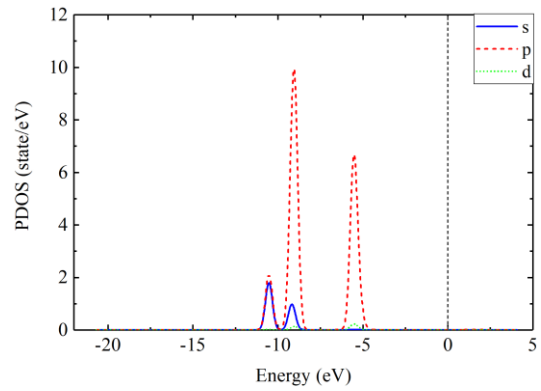
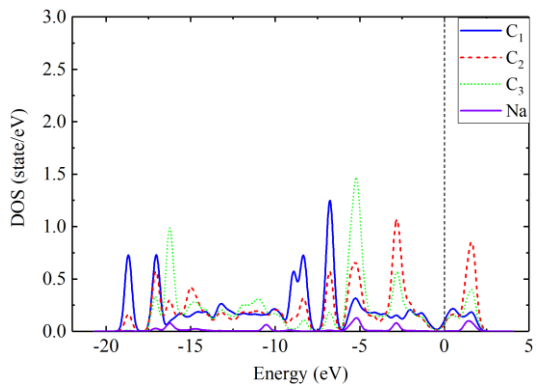
360 To further understand the nature of the interaction between the CO<sub>2</sub> molecule and the structure,  
 361 the PDOS diagrams of CO<sub>2</sub> adsorbed on the pristine and modified GDY structures are  
 362 displayed in **Fig. 9**. The contribution of each type of structural carbon atom, as well as  
 363 modifying atoms (N, Na), and CO<sub>2</sub> in the states, was taken into account in these images.



(a)

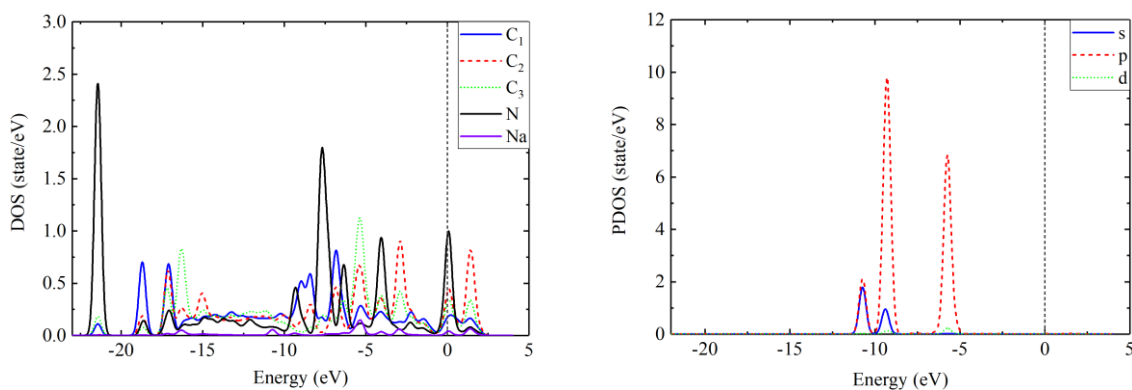


(b)



(c)





(d)

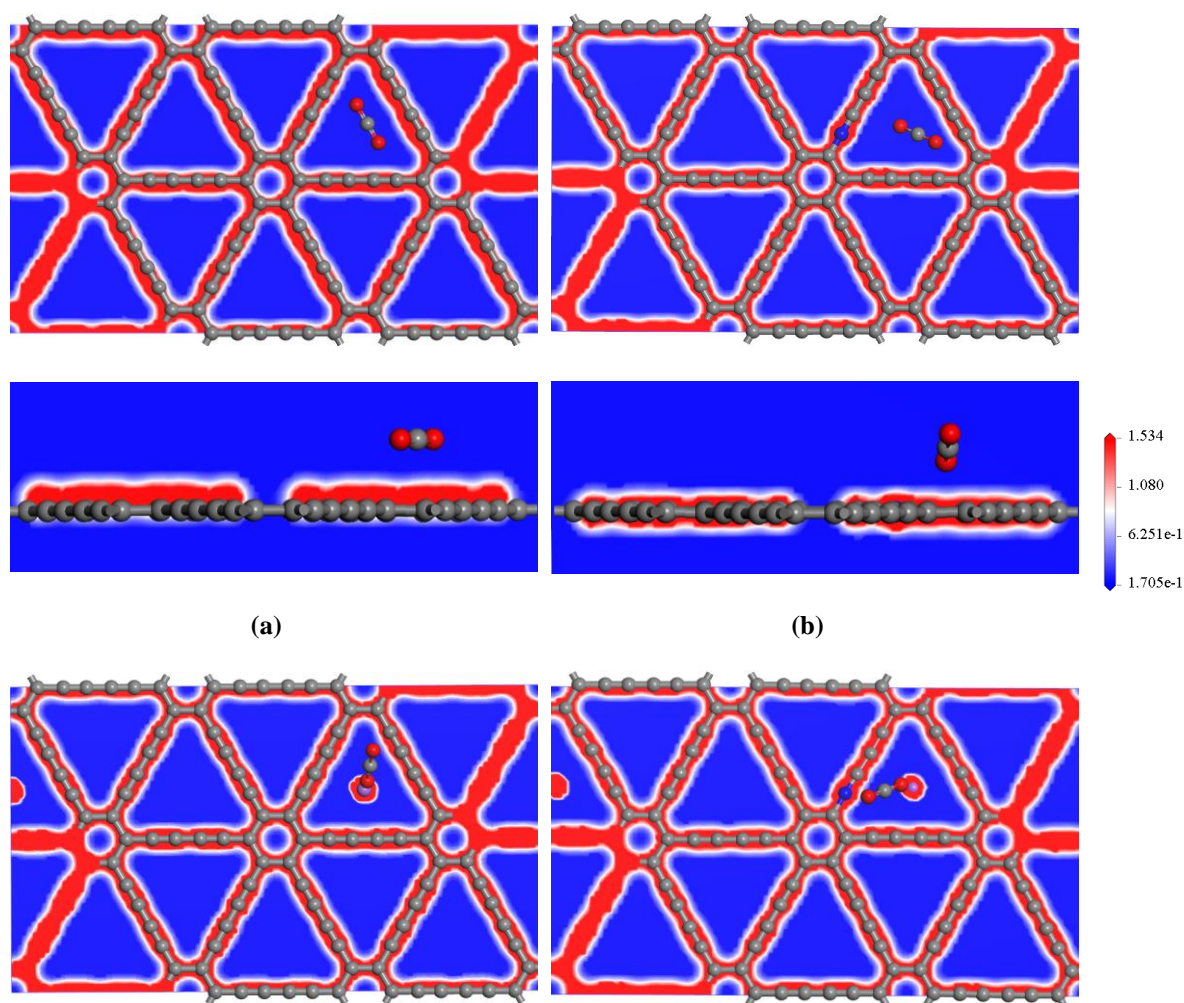
364 **Fig. 9.** PDOS images of the CO<sub>2</sub> adsorbed onto: (a) S1, (b) S2, (c) S3, and (d) S4 structures.

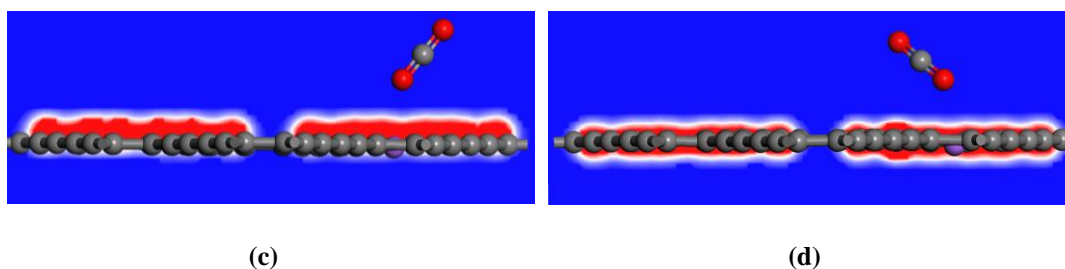
365

366 In the CO<sub>2</sub> molecule, the p-orbital contributes the most in states with two peaks in the energy  
 367 range of 3.5eV and 7eV. As a preliminary conclusion, these peaks in structures decorated with  
 368 Na atoms (S3 and S4) are in the lower energy range due to the Na atom's high electro-positivity.  
 369 Unlike the smaller peak, having higher overlapping with the electrons of all three types of  
 370 carbon atoms, the larger peak in the GDY structure has less overlap with the electrons of the  
 371 carbon atom in its energy domain. The overlapping of the orbitals of the CO<sub>2</sub> molecule and the  
 372 adsorbent, as observed in the PDOS of modified structures, could enhance the adsorbent  
 373 performance in the adsorption of CO<sub>2</sub> gas molecules.

374 The distribution of p orbital electrons in the CO<sub>2</sub> molecule has changed in S2 compared to S1,  
 375 and the height of the bigger (smaller) peak has decreased (increased), in addition to shifting the  
 376 peaks to lower energy levels. In the S2 configuration, GDY's structural electrons overlap with  
 377 the electrons of the N atom and the CO<sub>2</sub> molecule, increasing the released energy during the  
 378 CO<sub>2</sub> adsorption process. Electrons of the s- and p-orbitals of the CO<sub>2</sub> molecule overlap with  
 379 the electrons of the Na atom, as shown in **Figs. 9-(c) and 9-(d)**, enhancing the adsorption  
 380 energy. The reduced overlap of electrons of structural carbon atoms and the CO<sub>2</sub> gas molecule

381 in the S4 is related to the altered electron distribution in the carbon atoms (due to the presence  
382 of the N atom). This is why the S3 structure adsorbs CO<sub>2</sub> molecules better than the S4 structure.  
383 **Fig. 10** depicts the differences in each electron-density distribution of structure to provide  
384 additional evidence for the CO<sub>2</sub> capturing results. The blue and red regions in **Fig. 10** show  
385 electron depletion and enhancement, respectively. The white lines between the blue and red  
386 regions indicate a slight change in electron density. As can be seen, the presence of Na at the  
387 H3 position creates an electron enhancement area in the adsorbent structure, resulting in a  
388 secondary electric field. As a result of their higher interaction with CO<sub>2</sub>, S3 and S4 structures  
389 are better suited for trapping gas molecules.





390 **Fig. 10.** The difference electron density images of adsorbed CO<sub>2</sub> onto (a) S1, (b) S2, (c) S3, and (d) S4  
 391 structures.

392

### 393 **3.3. Capture capacity of CO<sub>2</sub> molecules onto the pristine and modified GDY**

394 After geometry optimization of the S1-S4 structures, all the possibilities for adsorption of the  
 395 first CO<sub>2</sub> were investigated. Afterward, the most stable configuration was used for placing the  
 396 second CO<sub>2</sub>. Again, all the possible positions for the adsorption of the second CO<sub>2</sub> were  
 397 considered, and this procedure was repeated for the adsorption of all the CO<sub>2</sub> molecules. The  
 398 amount of CO<sub>2</sub> the absorbent captures is a crucial consideration for determining the best  
 399 structure. CO<sub>2</sub> molecules were subsequently introduced to the structures to assess the  
 400 performance of the adsorbents from the standpoint of CO<sub>2</sub> capture. The system (adsorbent+  
 401 nCO<sub>2</sub>) was optimized at each stage, and the average adsorption energy ( $E_{ads}$ ) and phase  
 402 adsorption energy ( $E_s$ ) were computed. The US Department of Energy has set the energy value  
 403  $E_s=0.1\text{eV}$  as a criterion for determining the maximum amount of CO<sub>2</sub> adsorption capability.  
 404 Thus, to estimate the maximum adsorption capacity of each structure, placing the CO<sub>2</sub> molecule  
 405 on the structure continued until the  $E_s$  of the step became less than this threshold energy. The  
 406  $E_{ads}$  and  $E_s$ , C-O bond length, O-C-O angle, and hydrogen storage capacity (Wt %) for all four  
 407 structures are listed in **Table 6**.

408

409 **Table 6.**  $E_{\text{ads}}$  and  $E_{\text{s}}$  (eV), C-O bond length ( $L_{\text{C-O}}$ ), O-C-O angle, and maximum  $\text{CO}_2$  capture capacity (wt. %) in  
 410 S1, S2, S3, and S4 structures.

Struc.	# $\text{CO}_2$	$E_{\text{ads}}$ (eV)	$E_{\text{s}}$ (eV)	$L_{\text{C-O}}$ (Å)	$\angle\text{O-C-O}$	Wt. %	Struc.	# $\text{CO}_2$	$E_{\text{ads}}$ (eV)	$E_{\text{s}}$ (eV)	$L_{\text{C-O}}$ (Å)	$\angle\text{O-C-O}$	Wt. %
S1	1	-0.232	-0.232	$\frac{1.175}{1.175}$	179.646	44.87%	S3	1	-0.432	-0.432	$\frac{1.179}{1.167}$	179.283	52.46%
	2	-0.207	-0.183	$\frac{1.175}{1.175}$	179.631			2	-0.427	-0.421	$\frac{1.180}{1.166}$	179.586	
	3	-0.228	-0.269	$\frac{1.175}{1.175}$	179.253			3	-0.405	-0.361	$\frac{1.180}{1.169}$	178.763	
	4	-0.227	-0.224	$\frac{1.176}{1.174}$	179.193			4	-0.378	-0.299	$\frac{1.176}{1.173}$	179.889	
	5	-0.199	-0.090	$\frac{1.177}{1.175}$	179.730			5	-0.384	-0.407	$\frac{1.179}{1.169}$	179.342	
S2	1	-0.271	-0.271	$\frac{1.176}{1.174}$	179.173	68.92%	S4	6	-0.363	-0.259	$\frac{1.176}{1.174}$	179.796	59.34%
	2	-0.344	-0.416	$\frac{1.176}{1.174}$	179.079			7	-0.325	-0.098	$\frac{1.170}{1.177}$	179.197	
	3	-0.304	-0.226	$\frac{1.175}{1.176}$	179.288			1	-0.442	-0.442	$\frac{1.167}{1.181}$	179.214	
	4	-0.285	-0.227	$\frac{1.176}{1.175}$	179.134			2	-0.424	-0.406	$\frac{1.169}{1.179}$	178.855	
	5	-0.268	-0.199	$\frac{1.176}{1.175}$	179.753			3	-0.442	-0.367	$\frac{1.176}{1.173}$	179.653	
	6	-0.255	-0.191	$\frac{1.176}{1.175}$	179.678			4	-0.387	-0.223	$\frac{1.177}{1.169}$	179.870	
	7	-0.293	-0.230	$\frac{1.176}{1.174}$	179.784			5	-0.396	-0.432	$\frac{1.176}{1.173}$	179.565	
	8	-0.246	-0.209	$\frac{1.176}{1.174}$	179.741		6	-0.401	-0.424	$\frac{1.167}{1.180}$	178.628		
	9	-0.236	-0.158	$\frac{1.176}{1.174}$	179.665		7	-0.434	-0.238	$\frac{1.167}{1.180}$	178.628		
	10	-0.233	-0.206	$\frac{1.175}{1.175}$	179.553		8	-0.334	-0.230	$\frac{1.177}{1.173}$	179.648		
	11	-0.232	-0.220	$\frac{1.176}{1.174}$	179.371		9	-0.307	-0.096	$\frac{1.172}{1.177}$	179.324		
	12	-0.221	-0.093	$\frac{1.178}{1.173}$	179.195								

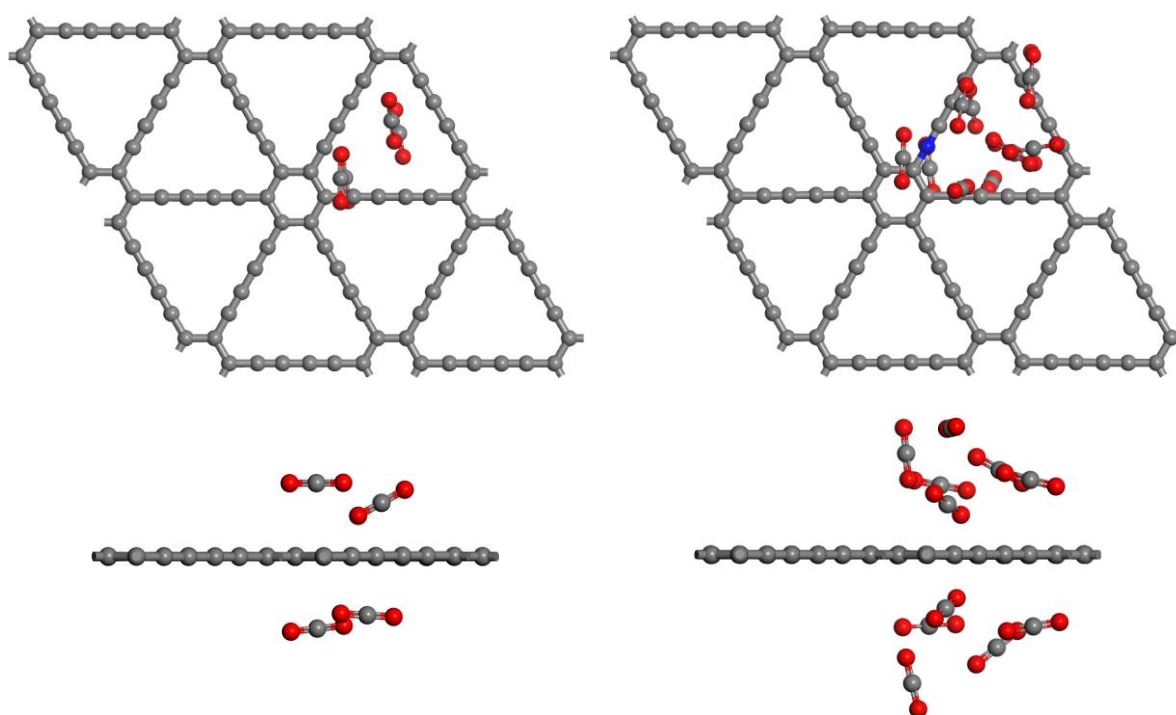
411

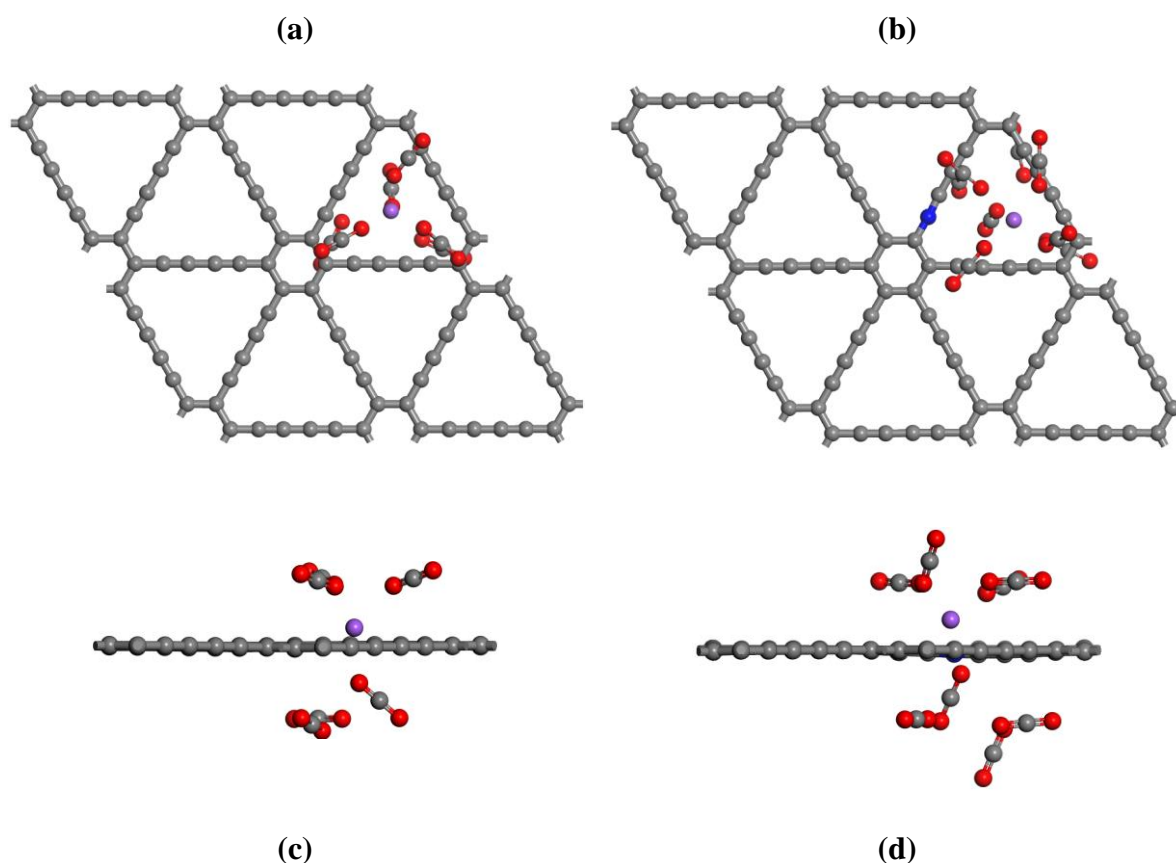
412 As previously reported, the bond length and angle of the free  $\text{CO}_2$  molecule are determined to  
 413 be 1.175Å and 179.66°, respectively. However, as seen during  $\text{CO}_2$  capture, the bond length  
 414 and angle of each  $\text{CO}_2$  molecule vary and vary around the values observed for free  $\text{CO}_2$ . The  
 415 number of  $\text{CO}_2$  molecules adsorbed in each of the structures S1, S2, S3, and S4 is 4, 11, 6, and  
 416 8, corresponding to about 44.87, 68.92, 59.34, and 58.16 Wt%, respectively. After the final

417 CO<sub>2</sub> molecule was placed in the structure and the system was optimized, the energy released  
418 by S1, S2, S3, and S4 was -0.090, -0.093, -0.098, and -0.096eV, respectively; this indicates  
419 that the adsorbents' maximum CO<sub>2</sub> capture capability has been reached.

420 As shown in **Table 6**, doping N atoms inside the structure increases the CO<sub>2</sub> capture capacity  
421 of the system by up to 1.5 times that of pure GDY. Although adding the Na atom to both the  
422 S1 and S2 structures improves the adsorption capacity compared to the S1, the S2 structure is  
423 a more storage-efficient structure obtained simply by doping the N atom onto the GDY. As  
424 seen in **Fig. 10**, adorning the Na atom in the structure results in the formation of an electron  
425 depletion zone, which can generate a secondary electric field in addition to the primary electric  
426 field of the structure. As a result of the influence of the field on the CO<sub>2</sub> molecules during the  
427 capturing process, the number of molecules captured in the adsorption site increased. **Fig. 11**  
428 depicts the final CO<sub>2</sub>-saturated system for all four structures (S1, S2, S3, and S4), and the state  
429 of the CO<sub>2</sub> molecules on either side of the adsorbents.

430



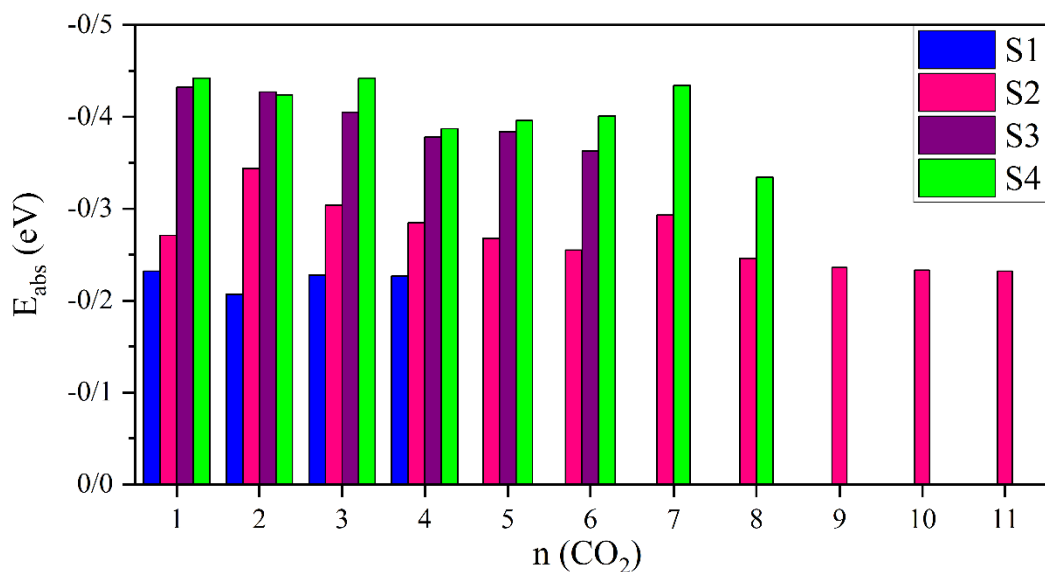


431 **Fig. 11.** Top and side views of the CO<sub>2</sub> storage of (a) S1-4CO<sub>2</sub>, (b) S2-11CO<sub>2</sub>, (c) S3-6CO<sub>2</sub>, and (d) S4-8CO<sub>2</sub>-  
 432 systems.

433

434 **Fig. 12** compares the CO<sub>2</sub> adsorption capacities of the structures with the adsorption energy  
 435 expressed in terms of the number of adsorbed molecules. As can be observed, following the  
 436 adsorption of the fourth CO<sub>2</sub> molecule with the adsorption energy of -0.227eV, the structure of  
 437 S1 is saturated. The doped N atom in the S2 structure enhances the CO<sub>2</sub> adsorption capacity  
 438 about threefold (11CO<sub>2</sub>), with a final adsorption energy of -0.232eV. In the S3, the Na-  
 439 decorating increases the amount of adsorbed CO<sub>2</sub> molecules up to 1.5 times, with a final  
 440 adsorption energy of -0.363eV. However, the number of adsorbed molecules improved for the  
 441 S4 structure by up to twofold, having a slightly lower final adsorption energy (-0.334eV).

442



443 **Fig. 12.** Comparison of the mean adsorption energy of each step against the number of CO<sub>2</sub> molecules for S1,  
 444 S2, S3, and S4 structures.

445

#### 446 **4. Conclusion**

447 The DFT-D2 approach was used to investigate the impacts of modifications such as N-doping,  
 448 Na-decoration and their combination on the structural and electronic properties of GDY as well  
 449 as the adsorption behavior of single CO<sub>2</sub>. By substituting N for the C2 atom, the best N-doped  
 450 GDY is obtained ( $E_{\text{coh}} = -7.231\text{eV}$ ), and by inserting a Na atom in the H3 site, the most stable  
 451 Na-decorated GDY is obtained ( $E_{\text{ads}} = -3.804\text{eV}$ ). H3 was also shown to be the optimal site for  
 452 Na-decorating with  $E_{\text{ads}} = -0.432\text{eV}$ . The electronic properties of all structures were also  
 453 investigated, including TDOS and band structures and atomic charge. To explore single CO<sub>2</sub>  
 454 capture, CO<sub>2</sub> molecules were initially positioned horizontally and vertically in the pristine and  
 455 best-modified GDY structure at H1, H2, H3, B, and M locations. The results indicated that for  
 456 S1, S2, and S3, H3 is the optimal site, whereas M is the optimal site for CO<sub>2</sub> adsorption on S4.  
 457 Also, the maximum value of adsorption energy was equal to about ( $40\text{ kJ}\cdot\text{mol}^{-1}$ ), which is

458 assumed that the adsorption of CO<sub>2</sub> on the nanosheets is physical and driven by Vander Waals  
459 forces [43].

460 Finally, each structure's maximal CO<sub>2</sub> capture capacity was determined by bringing CO<sub>2</sub>  
461 molecules close to the adsorbent and optimizing the resulting system. The results of this section  
462 indicate that S2 (N-doped GDY) has almost threefold the CO<sub>2</sub> capturing capability of S1  
463 (pristine GDY); thus, it is a candidate for future CO<sub>2</sub> capture, storage, detection, and removal  
464 applications.

465

#### 466 **Acknowledgments**

467 M. A.B. and Z. B. are grateful to the Research Council of the Lorestan University.

468

#### 469 **References**

- 470 [1] Gurkan B, Goodrich BF, Mindrup EM, Ficke LE, Massel M, Seo S, et al. Molecular  
471 design of high capacity, low viscosity, chemically tunable ionic liquids for CO<sub>2</sub>  
472 capture. *J Phys Chem Lett* 2010;1:3494–9.
- 473 [2] Venkataramanan NS, Suvitha A, Mizuseki H, Kawazoe Y. Functionalized  
474 Nanofullerenes for Hydrogen Storage: A Theoretical Perspective. *ArXiv Prepr*  
475 *ArXiv11064524* 2011.
- 476 [3] Li J, Hou M, Chen Y, Cen W, Chu Y, Yin S. Enhanced CO<sub>2</sub> capture on graphene via  
477 N, S dual-doping. *Appl Surf Sci* 2017;399:420–5.
- 478 [4] Darvishnejad MH, Reisi-Vanani A. Synergetic effects of metals in graphyne 2D  
479 carbon structure for high promotion of CO<sub>2</sub> capturing. *Chem Eng J* 2021;406:126749.



- 480 [5] Zou L, Zhu Y, Cen W, Jiang X, Chu W. N-doping in graphdiyne on embedding of  
481 metals and its effect in catalysis. *Appl Surf Sci* 2021;557:149815.
- 482 [6] Gu H, Zhong L, Shi G, Li J, Yu K, Li J, et al. Graphdiyne/Graphene Heterostructure:  
483 A Universal 2D Scaffold Anchoring Monodispersed Transition-Metal Phthalocyanines  
484 for Selective and Durable CO<sub>2</sub> Electroreduction. *J Am Chem Soc* 2021.
- 485 [7] Luo G, Qian X, Liu H, Qin R, Zhou J, Li L, et al. Quasiparticle energies and excitonic  
486 effects of the two-dimensional carbon allotrope graphdiyne: Theory and experiment.  
487 *Phys Rev B* 2011;84:75439.
- 488 [8] Zhang S, Du H, He J, Huang C, Liu H, Cui G, et al. Nitrogen-doped graphdiyne  
489 applied for lithium-ion storage. *ACS Appl Mater Interfaces* 2016;8:8467–73.
- 490 [9] Sun C, Searles DJ. Lithium storage on graphdiyne predicted by DFT calculations. *J*  
491 *Phys Chem C* 2012;116:26222–6.
- 492 [10] Wang S, Yi L, Halpert JE, Lai X, Liu Y, Cao H, et al. A novel and highly efficient  
493 photocatalyst based on P25--graphdiyne nanocomposite. *Small* 2012;8:265–71.
- 494 [11] Liu T, Wang Q, Wang G, Bao X. Electrochemical CO<sub>2</sub> reduction on graphdiyne: a  
495 DFT study. *Green Chem* 2021;23:1212–9.
- 496 [12] Li G, Li Y, Liu H, Guo Y, Li Y, Zhu D. Architecture of graphdiyne nanoscale films.  
497 *Chem Commun* 2010;46:3256–8.
- 498 [13] Niaei AHF, Hussain T, Hankel M, Searles DJ. Sodium-intercalated bulk graphdiyne as  
499 an anode material for rechargeable batteries. *J Power Sources* 2017;343:354–63.
- 500 [14] Jiao Y, Du A, Hankel M, Zhu Z, Rudolph V, Smith SC. Graphdiyne: a versatile  
501 nanomaterial for electronics and hydrogen purification. *Chem Commun*  
502 2011;47:11843–5.

- 503 [15] Ebadi M, Reisi-Vanani A. Methanol and carbon monoxide sensing and capturing by  
504 pristine and Ca-decorated graphdiyne: A DFT-D2 study. *Phys E Low-Dimensional*  
505 *Syst Nanostructures* 2021;125:114425.
- 506 [16] Wu Y, Chen X, Weng K, Jiang J, Ong W-J, Zhang P, et al. Highly Sensitive and  
507 Selective Gas Sensor Using Heteroatom Doping Graphdiyne: A DFT Study. *Adv*  
508 *Electron Mater* 2021:2001244.
- 509 [17] Li J, Zhong L, Tong L, Yu Y, Liu Q, Zhang S, et al. Atomic Pd on  
510 graphdiyne/graphene heterostructure as efficient catalyst for aromatic nitroreduction.  
511 *Adv Funct Mater* 2019;29:1905423.
- 512 [18] Kosar N, Shehzadi K, Ayub K, Mahmood T. Theoretical study on novel superalkali  
513 doped graphdiyne complexes: unique approach for the enhancement of electronic and  
514 nonlinear optical response. *J Mol Graph Model* 2020;97:107573.
- 515 [19] Xu P, Na N, Mohamadi A. Investigation the application of pristine graphdiyne (GDY)  
516 and boron-doped graphdiyne (BGDY) as an electronic sensor for detection of  
517 anticancer drug. *Comput Theor Chem* 2020;1190:112996.
- 518 [20] Ebadi M, Reisi-Vanani A, Houshmand F, Amani P. Calcium-decorated graphdiyne as  
519 a high hydrogen storage medium: evaluation of the structural and electronic properties.  
520 *Int J Hydrogen Energy* 2018;43:23346–56.
- 521 [21] Feng Z, Tang Y, Ma Y, Li Y, Dai Y, Ding H, et al. Theoretical investigation of CO<sub>2</sub>  
522 electroreduction on N (B)-doped graphdiyne monolayer supported single copper  
523 atom. *Appl Surf Sci* 2021;538:148145.
- 524 [22] Darvishnejad MH, Reisi-Vanani A. Multiple CO<sub>2</sub> capture in pristine and Sr-decorated  
525 graphyne: A DFT-D3 and AIMD study. *Comput Mater Sci* 2020;176:109539.

- 526 [23] Yang C, Wang Y, Yu J, Cao S. Ultrathin 2D/2D Graphdiyne/Bi<sub>2</sub>WO<sub>6</sub> Heterojunction  
527 for Gas-Phase CO<sub>2</sub> Photoreduction. *ACS Appl Energy Mater* 2021;4:8734–8.
- 528 [24] Dang Y, Guo W, Zhao L, Zhu H. Porous carbon materials based on graphdiyne basis  
529 units by the incorporation of the functional groups and Li atoms for superior CO<sub>2</sub>  
530 capture and sequestration. *ACS Appl Mater & Interfaces* 2017;9:30002–13.
- 531 [25] Bie C, Cheng B, Ho W, Li Y, Macyk W, Ghasemi JB, et al. Graphdiyne-based  
532 photocatalysts for solar fuel production. *Green Chem* 2022;24:5739–54.  
533 <https://doi.org/10.1039/d2gc01684b>.
- 534 [26] Perdew JP, Burke K, Ernzerhof M. Generalized gradient approximation made simple.  
535 *Phys Rev Lett* 1996;77:3865.
- 536 [27] Delley B. Hardness conserving semilocal pseudopotentials. *Phys Rev B*  
537 2002;66:155125.
- 538 [28] Delley B. From molecules to solids with the DMol 3 approach. *J Chem Phys*  
539 2000;113:7756–64.
- 540 [29] Akbari F, Reisi-Vanani A, Darvishnejad MH. DFT study of the electronic and  
541 structural properties of single Al and N atoms and Al-N co-doped graphyne toward  
542 hydrogen storage. *Appl Surf Sci* 2019;488:600–10.
- 543 [30] Ehrlich S, Moellmann J, Reckien W, Bredow T, Grimme S. System-dependent  
544 dispersion coefficients for the DFT-D3 treatment of adsorption processes on ionic  
545 surfaces. *ChemPhysChem* 2011;12:3414–20.
- 546 [31] Grimme S, Antony J, Ehrlich S, Krieg H. A consistent and accurate ab initio  
547 parametrization of density functional dispersion correction (DFT-D) for the 94  
548 elements H-Pu. *J Chem Phys* 2010;132:154104.

- 549 [32] Grimme S. Semiempirical GGA-type density functional constructed with a long-range  
550 dispersion correction. *J Comput Chem* 2006;27:1787–99.
- 551 [33] Monkhorst HJ, Pack JD. Special points for Brillouin-zone integrations. *Phys Rev B*  
552 1976;13:5188.
- 553 [34] Harrison RW, Lee WE. Processing and properties of ZrC, ZrN and ZrCN ceramics: a  
554 review. *Adv Appl Ceram* 2016;115:294–307.
- 555 [35] Lombardi EB, Mainwood A, Osuch K, Reynhardt EC. Computational models of the  
556 single substitutional nitrogen atom in diamond. *J Phys Condens Matter* 2003;15:3135–  
557 49. <https://doi.org/10.1088/0953-8984/15/19/314>.
- 558 [36] Li C, Li J, Wu F, Li SS, Xia JB, Wang LW. High capacity hydrogen storage in Ca  
559 decorated graphyne: A first-principles study. *J Phys Chem C* 2011;115:23221–5.  
560 <https://doi.org/10.1021/jp208423y>.
- 561 [37] Hu L, Hu X, Wu X, Du C, Dai Y, Deng J. Density functional calculation of transition  
562 metal adatom adsorption on graphene. *Phys B Condens Matter* 2010;405:3337–41.  
563 <https://doi.org/10.1016/j.physb.2010.05.001>.
- 564 [38] He F. Basic Structure and Band Gap Engineering: Theoretical Study of GDYs.  
565 Graphdiyne Fundamentals Appl. Renew. Energy Electron., John Wiley & Sons, Ltd;  
566 2022, p. 13–77. <https://doi.org/https://doi.org/10.1002/9783527828470.ch2>.
- 567 [39] Liu X, Wang Z, Tian Y, Zhao J. Graphdiyne-Supported Single Iron Atom: A  
568 Promising Electrocatalyst for Carbon Dioxide Electroreduction into Methane and  
569 Ethanol. *J Phys Chem C* 2020;124:3722–30. <https://doi.org/10.1021/acs.jpcc.9b11649>.
- 570 [40] S. sheng L. Semiconductor Physical Electronics. *Semicond Phys Electron* 2006.  
571 <https://doi.org/10.1007/0-387-37766-2>.

- 572 [41] Guillory JK. Book Review of CRC Handbook of Chemistry and Physics. 2009.
- 573 [42] Enejekwu FM, Ezeh CI, George MW, Xu M, Do H, Zhang Y, et al. A comparative  
574 study of mechanisms of the adsorption of CO<sub>2</sub> confined within graphene--MoS<sub>2</sub>  
575 nanosheets: a DFT trend study. *Nanoscale Adv* 2019;1:1442–51.
- 576 [43] Mahmood Aljamali N, Obaid Alfatlawi I. Physical and Chemical Adsorption and its  
577 Applications. *Int J Thermodyn Chem Kinet* 2021;7. <https://doi.org/10.37628/IJTCK>.
- 578